

Probing the structure and dynamics of molecular clusters using rotational wavepackets

¹Gediminas Galinis, ²Cephrise Cacho, ²Richard T. Chapman, ³Andrew M. Ellis, ⁴Marius Lewerenz, ¹Luis G. Mendoza Luna, ⁵Russell S. Minns, ⁴Mirjana Mladenović, ⁶Arnaud Rouzée, ²Emma Springate, ²I. C. Edmond Turcu, ¹Mark J. Watkins, ¹Klaus von Haeften*
¹University of Leicester, Department of Physics & Astronomy, Leicester, LE1 7RH, United Kingdom
²Central Laser Facility, STFC Rutherford Appleton Laboratory, United Kingdom
³University of Leicester, Department of Chemistry, Leicester, LE1 7RH, United Kingdom
⁴Université Paris-Est, Laboratoire Modélisation et Simulation Multi Echelle, MSME UMR8208 CNRS, 5 bd Descartes, 77454 Marne-la-Vallée, France
⁵University of Southampton, Chemistry, Southampton, SO17 1BJ, United Kingdom and
⁶Max Born Institute, Max Born Strasse 2A, 12489 Berlin, Germany
(Dated: May 11, 2021)

The chemical and physical properties of molecular clusters can heavily depend on their size, which makes them very attractive for the design of new materials with tailored properties. Deriving the structure and dynamics of clusters is therefore of major interest in science. Weakly bound clusters can be studied using conventional spectroscopic techniques, but the number of lines observed is often too small for a comprehensive structural analysis. Impulsive alignment generates rotational wavepackets, which provides simultaneous information on structure and dynamics, as has been demonstrated successfully for *isolated molecules* [1–8]. Here, we apply this technique for the first time to *clusters* comprising of a molecule and a single helium atom. By forcing the population of high rotational levels in intense laser fields we demonstrate the generation of rich rotational line spectra for this system, establishing the highly delocalised structure and the coherence of rotational wavepacket propagation. Our findings enable studies of clusters of different sizes and complexity as well as incipient superfluidity effects using wavepacket methods.

The study of weakly bound clusters requires very low temperatures to allow their formation, implying the population of only the lowest quantum levels. Consequently, the features in conventional rotational microwave (MW) spectroscopy comprise only a few lines – often not enough for a comprehensive analysis of the structure [9]. In contrast, spectral features of variable complexity can be generated using impulsive alignment. In this method, a rotational wavepacket forms through the non-resonant interaction of an intense laser field with a molecule, aligning it in space [4]. Tuning the laser pulse duration and intensity controls the number of rotational eigenstates in the wavepackets. By following the evolution of alignment in time it is possible to map these eigenstates and explore the rotational dynamics. Given the equivalence of time and frequency-domain information, spectra com-

prising of few, or many, lines can be generated. This ability is also of advantage for the exploration of liquids where the wavepacket dynamics will be sensitive to dephasing. A particularly promising liquid to begin such studies is superfluid helium. Frequency-domain spectra of molecules embedded into large superfluid helium droplets show sharp rotational transitions, suggesting that wavepackets will not dephase [9, 10]. However, the recent attempt to impulsively align molecules in large helium droplets by Pentlehner *et al.* showed that this was not the case [11]. The findings remain unexplained.

This work was motivated to establish a bridge between free molecules and helium droplets. We chose to study clusters of acetylene (C_2H_2) and a single helium atom in order to reduce size and complexity to a minimum. Rotational spectroscopy (MW) of C_2H_2 has neither been performed in large helium droplets nor in small clusters before, one limitation being a lack of a permanent dipole moment needed in MW spectroscopy. Several potential energy surfaces for C_2H_2 -He nevertheless exist, allowing for comparison between experiment and theory [12–14].

A beam comprising small C_2H_2 -He clusters was generated in a pulsed, supersonic expansion and propagated through a vacuum apparatus [15]. To excite rotational wavepackets 300 fs laser pulses (pump) intersected the beam of clusters followed by 50 fs laser pulses (probe) to detect molecular alignment (Fig. 1). Control of the number of rotational levels excited in the wavepackets was achieved by variation of the intensity of the pump pulses between 5×10^{11} and 5×10^{12} Wcm^{-2} . The probe pulse had a constant intensity of 1×10^{15} Wcm^{-2} , sufficient to instantly break molecular bonds in a Coulomb explosion, thereby generating C^+ fragment ions. Their velocity vectors, carrying the molecular alignment information, were selectively detected in a velocity map imaging (VMI) spectrometer [16] whose detector plane was parallel to the polarisation plane of both laser beams (xy plane in Fig 1). The two-dimensional projection of the recoiling C^+ fragment directions and intensities was used to determine $\cos^2(\theta)$ for each position on the detector, where θ designates the angle between polarisation of the pump laser and the projected velocity vectors. The average over the entire detector area, $\langle \cos^2(\theta)_{2D} \rangle$, is propor-

* kvh6@le.ac.uk

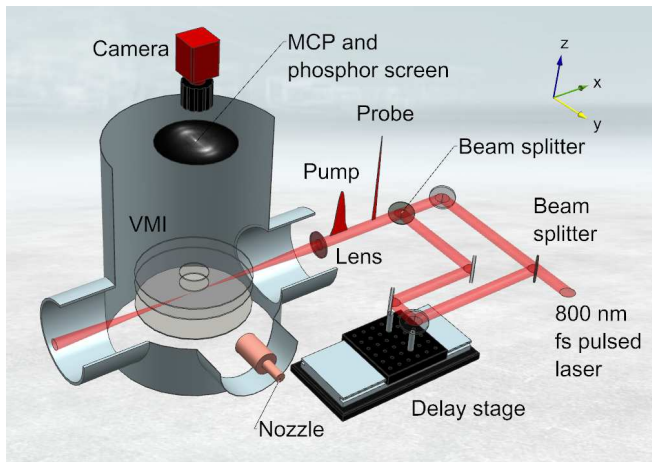


FIG. 1. **Schematic of experimental setup.** Helium- C_2H_2 clusters produced by expansion of 0.01 % C_2H_2 in 7 MPa He through a cooled Even-Lavie valve were irradiated by femtosecond pulses originating from a 30 fs, 1 kHz Ti:Sapphire laser operating at 800 nm (KM Labs Red Dragon). Both, pump and probe laser beams, comprising of separate grating compressors (not shown), were colinearly focused through a $f = 500$ mm lens into the molecular beam 50 mm downstream from the nozzle exit.

tional to the molecular alignment [5, 11]. This parameter was measured as a function of time by scanning the delay between pump and probe laser pulses to reveal the rotational dynamics of the clusters.

Fig. 2 shows raw Coulomb explosion images for C^+ under different expansion conditions. Fig. 2(a) shows the ion image under conditions where free C_2H_2 (no helium attached) is the dominant molecular species in the expanding gas. This particular image shows relatively sharp features, with evidence of more than one fragmentation channel leading to the formation of C^+ . By way of contrast, Fig. 2(b) shows the image obtained when the nozzle was cooled to 203 K to facilitate the formation of clusters. The angular distribution of the two images is identical, the only difference being higher kinetic energies in image (b). Increased kinetic energy unambiguously indicates the generation of further charges, although the laser parameters themselves have not changed. Space-charge effects can be excluded given that the temperature variation increases the gas number density in the interaction region only by 30 % – an insignificant reduction in the internuclear separation of ions in the gas compared to the high atomic number density within a cluster. We suspect that a mechanism, similar to that predicted for large helium droplets doped with Xe atoms, is operating for small clusters [17]. In our case the ionisation probability of He atoms might be enhanced by the presence of the solvated molecule.

The time-resolved molecular alignment, $\langle \cos^2(\theta)_{2D} \rangle$, is shown in Fig. 3 for conditions similar to Fig. 2(b). The strongest contribution originates from C_2H_2 whose full, half and quarter revivals reappear every rotational period

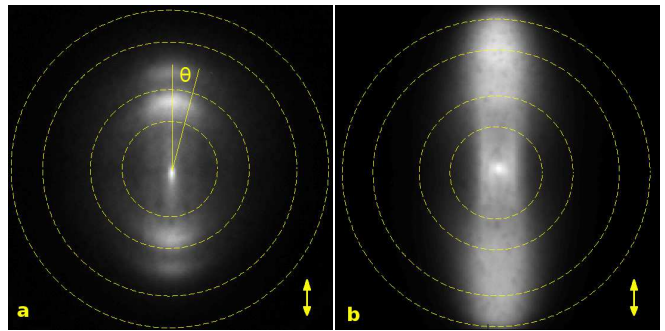


FIG. 2. **Velocity map images.** Images of the Coulomb explosion process obtained via velocity map imaging. These particular images focus on the C^+ fragment and were recorded with different nozzle temperatures, namely (a) 293 K and (b) 203 K, but under otherwise identical conditions. Production of clusters between helium and acetylene is enhanced in (b), supported by increased kinetic energy compared to (a). The yellow double-headed arrow indicates the direction of the pump and probe laser polarisations, which are parallel to the y -axis in Fig. 1. The dashed circles are guides to the eye.

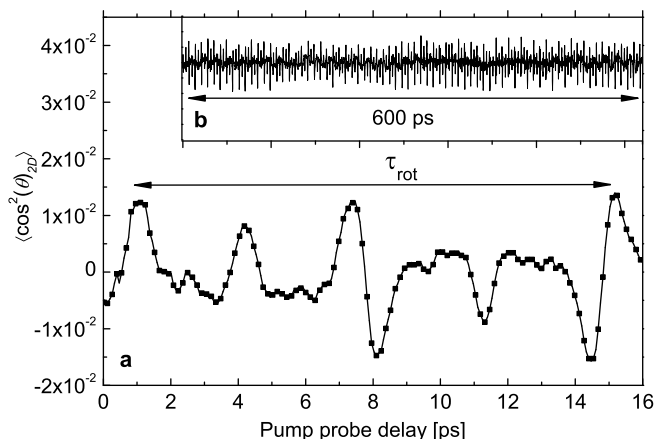


FIG. 3. **Time-resolved alignment.** (a) Rotational revivals obtained under conditions where the helium stagnation pressure and temperature were 6.4 MPa and 217 K, respectively. Note that the baseline has been subtracted. The data has been smoothed. The time difference between two full revivals is equal to the rotational period of acetylene and is indicated by a double-headed arrow. (b) For time delays up to the maximum of 600 ps, no decay in the amplitude, nor in the shape of the revivals, was observed. The coherence time of the wavepacket for free C_2H_2 molecules is therefore at least 600 ps.

as maximum alignment and anti-alignment. The features extend over the full range of the scan up to 600 ps without any appreciable decay in amplitude or shape, so one can infer that the coherence of the rotational wavepacket is at least 600 ps. Acetylene-helium cluster ($C_2H_2-He_n$) revivals are difficult to directly identify in the alignment scan. Therefore, a Fourier transform is performed, providing a much clearer picture.

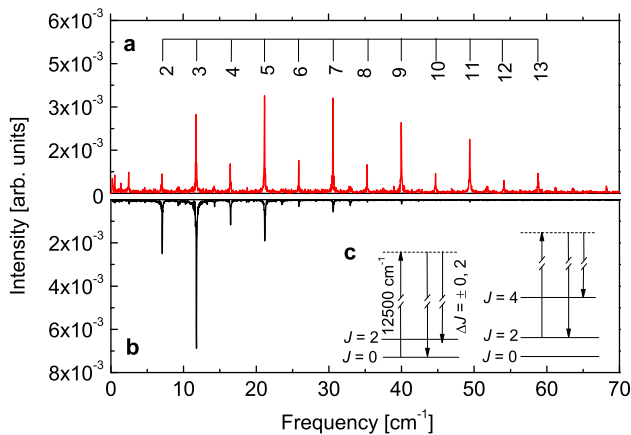


FIG. 4. **Overview spectra.** (a) Fourier transformation of the time-resolved molecular alignment recorded at a pump laser intensity of $5 \times 10^{12} \text{ Wcm}^{-2}$. (b) Spectrum recorded under similar conditions, but at a lower pump laser intensity of $5 \times 10^{11} \text{ Wcm}^{-2}$. The power spectra are dominated by strong peaks arising from beats between rotational levels of free C_2H_2 connected by $\Delta J = \pm 2$. The labels of the transitions correspond to the J quantum number of the final states, e.g. '2' labels the final state of the $J' = 2 \leftarrow J'' = 0$ excitation. (c) The rotational levels in the wavepacket are excited through sequential Raman excitations with an 800 nm ($12,500 \text{ cm}^{-1}$) laser pulse. This process sequentially populates higher levels via virtual states, as schematically illustrated in the inset. Odd J levels exhibit stronger lines because of the 3:1 population ratio controlled by nuclear spin statistics.

The Fourier transform of the time-resolved molecular alignment is shown for two different pump laser intensities in Fig. 4. A series of discrete lines is produced, which corresponds to particular frequency contributions of C_2H_2 to the rotational wavepacket. The strongest features seen in Fig. 4 coincide with the beat frequencies of C_2H_2 at $6B + 4nB$, where B is the C_2H_2 rotational constant ($B = 1.1769 \text{ cm}^{-1}$ [18]) and $n = 0, 1, 2, 3, \text{ etc.}$ Six members of this series are seen at the pump power of $5 \times 10^{11} \text{ Wcm}^{-2}$. The first line at $6B$ frequency is equivalent to the $J' = 2 \leftarrow J'' = 0$ transition, with successive lines at $10B, 14B, 18B, \text{ etc.}$ When the pump laser intensity is increased to $5 \times 10^{12} \text{ Wcm}^{-2}$, higher rotational transitions are induced, reaching up to the $J = 13$ rotational energy level.

In the low frequency range, shown in Fig. 5(a), several prominent peaks were observed which do not fit to the well-known rotational transitions for free C_2H_2 and are therefore attributed to $\text{C}_2\text{H}_2\text{-He}_n$ clusters. The full widths at half maximum of these features were found to be 0.03 cm^{-1} , which matches the experimental limit in resolution set by the length of the delay scan of 600 ps. Hence, the line width of the peaks assigned to $\text{C}_2\text{H}_2\text{-He}_n$ clusters is consistent with a coherence time for the rotational wavepacket of at least 600 ps. This first observation of coherent propagation of rotational wavepackets

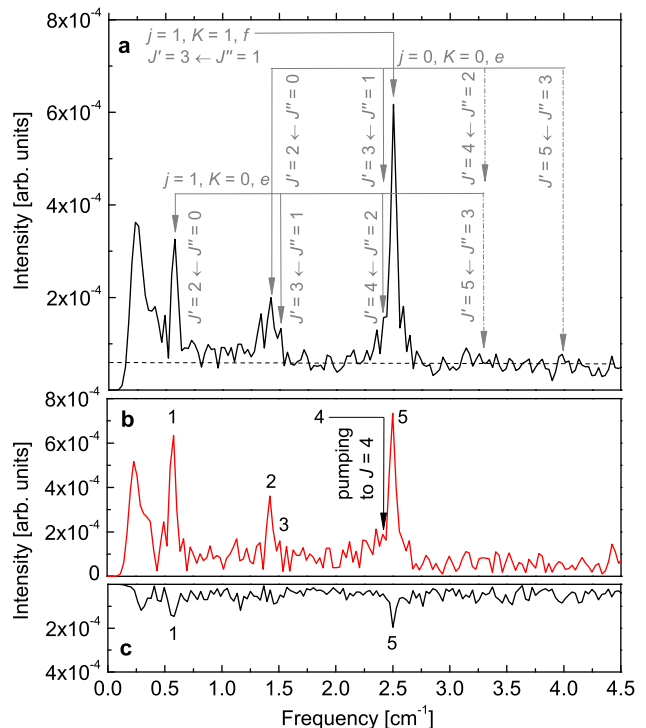


FIG. 5. **$\text{C}_2\text{H}_2\text{-He}$ spectrum and pump laser intensity dependence.** An average of five spectra recorded for similar expansion conditions is shown in panel (a). Possible, but not observed transitions are marked by dashed-dot arrows. The noise level, established through zero pumping power measurements, is indicated by a horizontal dashed line. Two spectra at two pump laser intensities of (b) 5×10^{12} and (c) $5 \times 10^{11} \text{ Wcm}^{-2}$. Prominent $\text{C}_2\text{H}_2\text{-He}$ features are annotated by numbers 1 - 5. The pump power dependence of the intensity of line '4' reflects sequential pumping $J' = 4 \leftarrow J'' = 2$.

in small $\text{C}_2\text{H}_2\text{-He}_n$ clusters contrasts with the strong dephasing found in large helium droplets. As detailed below we can assign some of the $\text{C}_2\text{H}_2\text{-He}_n$ features to the simplest cluster, $\text{C}_2\text{H}_2\text{-He}$.

To guide the assignment the interaction energies for this cluster were calculated over a wide range of structures using the coupled cluster singles and doubles with perturbative triples (CCSD(T)) method. The analytical potential energy surface was used to compute rovibrational energy levels and wave functions, as detailed in the supplementary information. Selected levels and transition energies from these calculations are displayed in Fig. 6 and collected in Table I. The computed rovibrational ground state energy is -7.417 cm^{-1} relative to the dissociation limit into $\text{C}_2\text{H}_2 + \text{He}$. Only the total angular momentum quantum number J and the parity of the wave functions are rigorous quantum numbers. Parity is coded by the symbols e and f for levels with parity $+(-1)^J$ and $-(-1)^J$, respectively. Inspection of the level structure and analysis of the wave functions reveals that the $\text{C}_2\text{H}_2\text{-He}$ does not behave like a linear molecule in

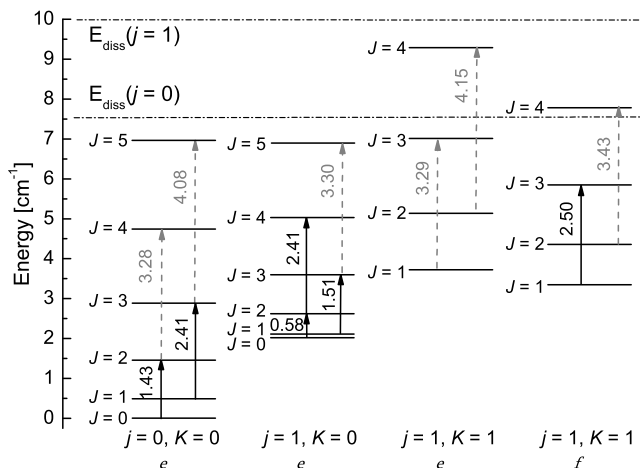


FIG. 6. **Rotational energy level diagram of C₂H₂-He.** The vertical arrows designate the transitions observed, whereas the dashed, grey arrows indicate possible but not observed transitions.

spite of its linear minimum energy structure. We can introduce another quantum number, j , which refers to the internal rotation of the C₂H₂ unit. Although approximate, this turns out to be a useful quantum number, which is consistent with the floppy character of the cluster, which is completely delocalised over the entire angular domain even in its rovibrational ground state. We additionally label the states by the approximate quantum number K for the projection of j onto the intermolecular axis.

TABLE I. Energy level assignment of measured lines. Quantum numbers of the initial states are denoted by j'' , K'' , J'' and of the final states by j' , K' , J' . The experimental line positions are given in cm⁻¹ and the estimated error margin in each case is ± 0.03 cm⁻¹. The transition labels in the first column are identical with the labels of the peaks in Fig. 5.

He-HCCH		j''	K''	J''	j'	K'	J'	Exp.	Calc.
1	<i>e</i>	1	0	0	1	0	2	0.58	0.60
3	<i>e</i>	1	0	1	1	0	3	1.51	1.49
4	<i>e</i>	1	0	2	1	0	4	2.41	2.41
2	<i>e</i>	0	0	0	0	0	2	1.43	1.46
4	<i>e</i>	0	0	1	0	0	3	2.41	2.40
5	<i>f</i>	1	1	1	1	1	3	2.50	2.50

Based on these results, five peaks at 0.58, 1.43, 1.51,

2.41 and 2.50 cm⁻¹ were assigned to C₂H₂-He, yielding an agreement between theory and experiment within 0.02 cm⁻¹. We note that the present calculation provides a better match to the measured line positions than the best potential energy surface available prior to this work [14]. The expected Raman transitions for C₂H₂-He are marked in Fig. 6 by vertical arrows and text, showing the energy differences in cm⁻¹. The assignment of the lines in the low frequency range is shown in Table I.

The identified C₂H₂-He features depend distinctly on the pump laser intensity as shown in Figs. 5(b) and (c). At lower pump intensity, two lines exceed the noise level, namely the lines assigned to the transitions $J' = 2 \leftarrow J'' = 0$ in the $j = 1$, $K = 0$, *e* manifold, labelled '1', and the $J' = 3 \leftarrow J'' = 1$ in the $j = 1$, $K = 1$, *f* manifold, labelled '5'. The intensities of these lines grow with increasing pump laser energy due to more clusters being excited. Additional lines emerge, for example the $J' = 2 \leftarrow J'' = 0$ transition in the $j = 0$, $K = 0$, *e* manifold, labelled '2'. Population transfer to higher lying states in the rotational wavepacket due to more intense pumping is also observed. In particular, the $J'' = 2$ state in the $j = 1$, $K = 0$, *e* manifold is pumped to the $J' = 4$ state, labelled '4'. Two further transitions, the $J' = 5 \leftarrow J'' = 3$ in the $j = 1$, $K = 0$, *e* and the $J' = 5 \leftarrow J'' = 3$ in the $j = 0$, $K = 0$, *e* manifold, indicated in Fig. 5(a) by dotted arrows, exhibit intensities within the noise level and cannot safely be established.

In conclusion, it has been shown for the first time that it is possible to construct a coherent rotational wavepacket for a weakly bound cluster between a molecule and a helium atom using impulsive alignment. The dynamics of this wavepacket was followed in the time domain using a second laser pulse, yielding features that can be subjected to Fourier transformation to yield the underlying rotational energy level structure. By this means we have established the highly delocalised, floppy structure of C₂H₂-He, a van der Waals cluster which is only bound by *ca.* 7 cm⁻¹. The observed rotational energy level structure is in excellent agreement with theoretical predictions.

Our observation enables the simultaneous determination of structure and dynamics in free atomic and molecular clusters, which is vital for the fundamental understanding of size-effects and interactions in condensed matter, for example, incipient superfluidity. This knowledge will ultimately be critical for the development of new materials with tailored properties, addressing the relevance of clusters in various applied disciplines, for example catalysis, solar cells, opto-electronics and biomedical imaging.

[1] Seideman, T. Revival structure of aligned rotational wave packets. *Phys. Rev. Lett.*, **83**, 4971–4974, (1999).

[2] Rosca-Pruna, F. & Vrakking, M. J. J. Experimental observation of revival structures in picosecond laser-induced

- alignment of I₂. *Phys. Rev. Lett.*, **87**, 153902 (2001).
- [3] Itatani, J. *et al.* Tomographic imaging of molecular orbitals. *Nature*, **432**, 867–871 (2004).
- [4] Seideman, T. and Hamilton, E. Nonadiabatic alignment by intense pulses. Concepts, theory, and directions. *Adv. Atom. Mol. Opt. Phys.*, **52**, 289–329 (2006).
- [5] Ghafur, O. *et al.* Impulsive orientation and alignment of quantum-state-selected NO molecules. *Nature Phys.*, **5**, 289–293 (2009).
- [6] Bisgaard, Ch. Z. *et al.* Time-resolved molecular frame dynamics of fixed-in-space CS₂ molecules. *Science*, **323**, 1464–1468 (2009).
- [7] Kanai, T., Minemoto, S. & Sakai, H. Quantum interference during high-order harmonic generation from aligned molecules. *Nature*, **435**, 470–474 (2005).
- [8] Velotta, R., Hay, N., Mason, M. B., Castillejo, M. & Marangos, J. P. High-order harmonic generation in aligned molecules. *Phys. Rev. Lett.*, **87**, 183901 (2001).
- [9] Surin L. A. *et al.* Rotational Study of Carbon Monoxide Solvated with Helium Atoms. *Phys. Rev. Lett.*, **101**, 233401 (2008).
- [10] Hartmann, M., Miller, R. E., Toennies, J. P. & Vilesov, A. F. Rotationally Resolved Spectroscopy of SF₆ in Liquid Helium Clusters: A Molecular Probe of Cluster Temperature. *Phys. Rev. Lett.*, **75**, 1566 (1995).
- [11] Pentlehner, D., Nielsen, J. H., Slenczka, A., Mølmer, K. & Stapelfeldt, H. Impulsive Laser Induced Alignment of Molecules Dissolved in Helium Nanodroplets. *Phys. Rev. Lett.*, **110**, 093002 (2013).
- [12] Moszynski, R., Wormer, P. E. S. & van der Avoird, A. Ab initio potential energy surface and near-infrared spectrum of the He-C₂H₂ complex. *J. Chem. Phys.*, **102**, 8385 (1995).
- [13] Rezaei, M., Moazzen-Ahmadi, N., McKellar, A. R. W., Fernández, B. & Farrelly, D. Towards an understanding of the helium–acetylene van der Waals complex. *Mol. Phys.*, **110**, 2743–2750 (2012).
- [14] Fernández, B., Henriksen, Ch. & Farrelly, D. Refined ab initio intermolecular ground-state potential energy surface for the He-C₂H₂ van der Waals complex. *Mol. Phys.*, **111**, 1173 (2013).
- [15] Even, U., Jortner, J., Noy, D., Lavie, N. & Cossart-Magos, C. Cooling of large molecules below 1 K and He cluster formation. *J. Chem. Phys.*, **112**, 8068 (2000).
- [16] Eppink, A. T. J. B. & Parker, D. H. Velocity map imaging of ions and electrons using electrostatic lenses: Application in photoelectron and photofragment ion imaging of molecular oxygen. *Rev. Sci. Instrum.*, **68**, 3477 (1997).
- [17] Mikaberidze, A., Saalmann, U. & Rost, J. M. Laser-driven nanoplasmas in doped helium droplets: Local ignition and anisotropic growth. *Phys. Rev. Lett.*, **102**, 128102 (2009).
- [18] Callomon, J. H. & Stoicheff, B. P. High resolution Raman spectroscopy of gases: VIII. Rotational spectra of acetylene, diacetylene, diacetylene-D₂, and dimethylacetylene. *Can. J. Phys.*, **35**, 373–382 (1957).
- Acknowledgements.* The authors wish to thank STFC for the funded access to the Artemis facility at the Rutherford Appleton Laboratory and the University of Leicester for funding to support the studentship associated with this project. Also we would like to thank S. Hook, P. Rice, N. Rodrigues and S. Thornton for technical support during the experiment as well as J. Underwood and M. Siano for their contributions to the design of the VMI spectrometer. KvH kindly acknowledges funding by STFC (seed corn fund for experiments using 4th generation light sources) and the Leverhulme Trust (F/00212/AH). RSM would like to thank the Royal Society for a University Research Fellowship (UF100047), ML and MM acknowledge computational resources funded through ANR grant ANR-08-BLAN-0146-01.
- Author contributions.* G. Galinis: prepared, set up and performed experiment, analysed and interpreted data and wrote the manuscript, C. Cacho: supported experiment, R. Chapman: prepared, set up and supported experiment, A. Ellis: set up and performed experiment, interpreted data and wrote manuscript, M. Lewerenz: performed theoretical work, analysed and interpreted data and wrote the manuscript, L. G. Mendoza Luna: set up and performed experiment, performed theoretical work, R. Minns: set up and performed experiment, analysed and interpreted data, M. Mladenovic: performed theoretical work, analysed and interpreted data, A. Rouzee: performed theoretical work and interpreted data, E. Springate: managed the laboratory and supported experiment, E. Turcu: ran the laser system and supported experiment, M. Watkins: set up and performed experiment, analysed and interpreted data, performed theoretical work and wrote the manuscript, K. von Haeften: lead the project, set up and performed experiment, interpreted data and wrote the manuscript (principal investigator). All authors edited and commented on the manuscript.
- Competing Financial Interest Statement.* All authors declare that there are no conflicts with regards to competing financial interests.

Supplementary information: Prediction of rovibrational states of C₂H₂-He

The C₂H₂ unit was fixed at its experimental ground state averaged geometry¹. The interaction energies between C₂H₂ and a helium atom were computed in a Jacobi coordinate system with a Jacobi vector R pointing from the centre of mass of C₂H₂ to the helium atom and a Jacobi angle θ enclosed between R and the C₂H₂ molecular axis. Total electronic energies were computed on a grid of 300 points covering $0 \leq \theta \leq 90^\circ$ in steps of 10° and a θ dependent radial grid typically ranging between 2.50 and 20 Å. We used the coupled cluster singles and doubles with perturbative triples, CCSD(T), method and included all 16 electrons in the correlation treatment. Core optimised correlation consistent augmented (doubly augmented for He) basis sets according to Dunning were employed as implemented in the MOLPRO electronic structure package². Total energies for the complex obtained with basis sets from triple zeta, (d)aug-cc-pCVTZ, to quintuple zeta, (d)aug-cc-pCV5Z, level were extrapolated to the complete basis limit using the procedure of Peterson et al.³. The extrapolated total energies were converted into interaction energies by subtracting the result of an extrapolation for $R = 100$ Å and $\theta = 0$. The grid point with the strongest interaction is at $R = 4.32$ Å and $\theta = 0$ with a potential value of $V_{int} = -25.100$ cm⁻¹ relative to separate monomers at $V = 0$. All 235 interaction energies below +200 cm⁻¹ were least squares fitted to an angle dependent extended Tang-Toennies⁴ form:

$$V_{int}(R, \theta) = A(\theta) \exp\{-[b_1(\theta)R + b_2(\theta)R^2]\} - \sum_{k=3,8} f_{2k}(b(\theta), R) \frac{C_{2k}(\theta)}{R^{2k}} \quad (1)$$

The radial parameters $X = A, b_1, b_2, C_6, C_8, C_{10}$ are expressed by even order Legendre series according to

$$X(\theta) = \sum_{l=0,2,\dots} X^{(l)} P_l(\theta) \quad (2)$$

Higher order coefficients $C_{2k}, k > 5$, are defined by the standard recursion $C_{2k+2} = (C_{2k}/C_{2k-2})^3 C_{2k-4}$ and the

functions f_{2k} are Tang-Toennies damping functions with $b(\theta) = b_1(\theta) + 2b_2(\theta)R$. The fitting model contains 24 free parameters and reproduces the ab initio interaction energies with a root mean square error of 0.039 cm⁻¹ and a largest deviation of 0.22 cm⁻¹. In atomic units the coefficients for this analytical representation have the following values:

$A^{(0)}$	0.1918812E+02	$C_6^{(0)}$	0.1248242E+02
$A^{(2)}$	0.2504029E+02	$C_6^{(2)}$	-0.2662071E+01
$A^{(4)}$	0.8700405E+01	$C_6^{(4)}$	-0.4200783E+01
$A^{(6)}$	0.1256556E+01	$C_6^{(6)}$	-0.5564107E+01
$b_1^{(0)}$	0.1327564E+01	$C_8^{(0)}$	0.1318068E+04
$b_1^{(2)}$	-0.3394156E+00	$C_8^{(2)}$	0.1819554E+04
$b_1^{(4)}$	-0.1268924E+00	$C_8^{(4)}$	0.8531615E+03
$b_1^{(6)}$	0.1446208E-01	$C_8^{(6)}$	0.1011623E+04
$b_2^{(0)}$	0.4538917E-01	$C_{10}^{(0)}$	-0.2223242E+05
$b_2^{(2)}$	0.4238423E-01	$C_{10}^{(2)}$	-0.2251989E+05
$b_2^{(4)}$	0.1040915E-01	$C_{10}^{(4)}$	-0.1157502E+05
$b_2^{(6)}$	-0.1945577E-02	$C_{10}^{(6)}$	-0.3578250E+05

Bound rovibrational levels for the fitted surface were calculated with the DVR-DGB method, which uses a discrete variable representation (DVR) for the angular coordinate and a distributed Gaussian basis (DGB) for the radial degree of freedom⁵. We used 51 Gauss-Legendre DVR points in θ and an angle dependent radial basis composed of up to 85 non-evenly distributed Gaussians between 2.1 and 160 Å. Energy eigenvalues and wave functions were computed for both parities and for total angular momentum $0 \leq J \leq 10$, but only levels up to $J = 5$ were found to be bound. Energy levels are converged to better than 0.001 cm⁻¹. The computed rovibrational ground state energy is -7.417 cm⁻¹. The computed level structure and the analysis of the wave functions shows that C₂H₂-He does not behave like a linear molecule in spite of its linear electronic minimum. Already in its rovibrational ground state the complex is completely delocalised over the entire angular domain.

¹ Herman, M., Campargue, A., Idrissi, M. I. E. & Van der Auwera, J. Vibrational Spectroscopic Database on Acetylene, $\tilde{X}^1\Sigma_g^+$ (¹²C₂H₂, ¹²C₂D₂ and ¹³C₂H₂) *J. Phys. Chem. Ref. Data*, **32**, 922 (2003).

² Werner, H. J. et al. MOLPRO, version 2012.1, a package of *ab initio* programs (2012), see <http://www.molpro.net>.

³ Peterson, K. A., Woon, D. E. & Dunning Jr., T. H. Benchmark calculations with correlated molecular wave functions. IV. The classical barrier height of the H+H₂ → H₂+H re-

action. *J. Chem. Phys.* **100**, 7410 (1994).

⁴ Tang, K. T. & Toennies, J. P. An improved simple model for the van der Waals potential based on universal damping functions for the dispersion coefficients. *J. Chem. Phys.* **80**, 3726 (1984).

⁵ Mladenović, M. & Bačić, Z. Rovibrational states of Ar-HCN van der Waals complex: A localized representation calculation. *J. Chem. Phys.* **94**, 4988 (1991).